Classification of Geophysical Basins Derived From SRTM and Cartosat DEMs via Directional Granulometries

Article *in* IEEE Journal of Selected Topics in Applied Earth Observations and Remote Sensing · December 2019

DOI: 10.1109/JSTARS.2019.2955986

CITATIONS
6

READS
35

2 authors:

K. Nagajothi
Indian Space Research Organization
10 PUBLICATIONS **32** CITATIONS
SEE PROFILE

B. S Daya Sagar
Indian Statistical Institute
123 PUBLICATIONS **758** CITATIONS
SEE PROFILE

Classification of Geophysical Basins Derived From SRTM and Cartosat DEMs via Directional Granulometries

Kannan Nagajothi, *Member, IEEE*, and B. S. Daya Sagar, *Senior Member, IEEE*

***Abstract*—Spatial patterns from terrestrial surfaces have great potential to better understand the surficial phenomena and processes. This article provides an approach for classification of the hierarchically partitioned basins, subbasins, and watersheds with respect to high-directional granulometric index, low-directional granulometric index, and global granulometric index. Grayscale global and directional granulometric indexes of basin and corresponding watersheds derived from Shuttle Radar Topographic Mission (SRTM) and Cartosat digital elevation models (DEMs) of the Lower Indus subbasin of peninsular India are computed. The end results shown are in the forms of watersheds categorized and classified according to global and high- and low-directional grayscale granulometric indexes. It is interesting to observe that the classification of watersheds derived from SRTM and Cartosat DEMs, respectively, yielded similar results, suggesting it would be worthwhile to explore the potential relationships between the directional granulometric indexes of the watersheds and their resistance to perturbations caused by endogenic and exogenic forces. It is also observed that the orientation of watersheds and the general flow direction within those watersheds are in the direction in which the watersheds yield high-directional granulometric index.**

***Index Terms*—Classification, digital elevation model (DEM), granulometries, mathematical morphology, subbasin, watershed.**

I. Introduction

SPATIAL patterns from terrestrial surficial data available in the forms of digital elevation models (DEMs) include valleys and ridges, peaks and pits, and basins and watersheds. The quantitative analyses of such terrestrial patterns provide clues about the terrestrial composition. Morphometric characterization of such surfaces has been done via fractal analysis [1]–[10]. One among the aforementioned patterns is the basins that are partitioned from the terrestrial surficial data. Traditional approaches employed in basin characterization include morphometric and hypsometric analyses. These analyses, respectively, require river networks and elevation contours usually traced from topographic maps. With the advent of DEM, mathematical morphology based algorithms provided novel ways to quantitatively characterizing basins that not only complement the classical morphometric analysis but many times also outperform it.

Terrestrial surficial data available in the form of DEMs depict elevation values in a normalized form at all spatial positions. DEMs are derived from remotely sensed satellite data acquired via either microwave or active/passive sensing mechanisms. Such remotely sensed satellite data paved ways to generate DEMs at multiple spatial and temporal scales by exploiting the stereoscopy and interferometry principles. Now very high resolution LiDAR DEMs, though expensive, are available. These DEMs provide a great tool for geoscientists in various fields of research such as quantitative analysis of complex geometric features, to understand the spatio–temporal behavior of terrestrial processes and visualization in a real-time mode. Though DEMs available for whole earth terrestrial and earth-like planetary surfaces, and they offer huge benefits for the geoscientific community, it is our view that these global scale DEMs have been underutilized in quantitative basin and watershed characterization. All branches of geosciences and geography would find DEMs immensely useful for better understanding the dynamics of terrestrial surfaces and processes [11]–[17].

DEM data of geophysical basins available across very fine to very coarse spatial and temporal scales are an excellent source to perform powerful computations to derive morphologically and geometrically significant information. Publicly available DEM data include Shuttle Radar Topographic Mission (SRTM) and Cartosat DEMs [18], [19]. These DEMs facilitate researchers to develop and apply robust algorithms to: 1) retrieve surficial features [20]–[33]; 2) classify of data [34]–[44]; 3) quantitatively characterize surficial roughness [45]–[47]; 4) carry out quantitative spatial planning [48]–[50]; and 5) model, simulate, and visualize the terrestrial surface processes [51]–[56]. Geophysical basins and watersheds derived from DEMs possess varied surficial complexities that have relationships with geometrical properties and geophysical functions and processes. We employed the directional structuring elements in our earlier studies related to automatic orientation detection of planar river basins (spatial objects). Directional structuring elements are popular in image analysis, but employed for the first time in this study on

Manuscript received May 18, 2019; revised August 23, 2019 and October 29, 2019; accepted November 21, 2019. Date of publication December 18, 2019; date of current version February 4, 2020. The work of B. S. D. Sagar was supported in part by the Department of Science and Technology-Science and Engineering Research Board (DST-SERB) under Grant EMR/2015/000853 SERB, in part by the Indian Space Research Organisation (ISRO) under Grant ISRO/SSPO/Ch-1/2016-17, and in part by DST-ITPAR-IV under Grant INT/Italy/ITPAR-IV/Telecommunication/2018. *(Corresponding author: B. S. Daya Sagar.)*

K. Nagajothi is with the Regional Remote Sensing Centre-South, Indian Space Research Organisation, Bangalore 560037, India (e-mail: nagajothik@gmail.com).

B. S. Daya Sagar is with the Systems Science and Informatics Unit, Indian Statistical Institute, Bangalore 560059, India (e-mail: bsdsagar@isibang.ac.in).

Color versions of one or more of the figures in this article are available online at http://ieeexplore.ieee.org.

Digital Object Identifier 10.1109/JSTARS.2019.2955986

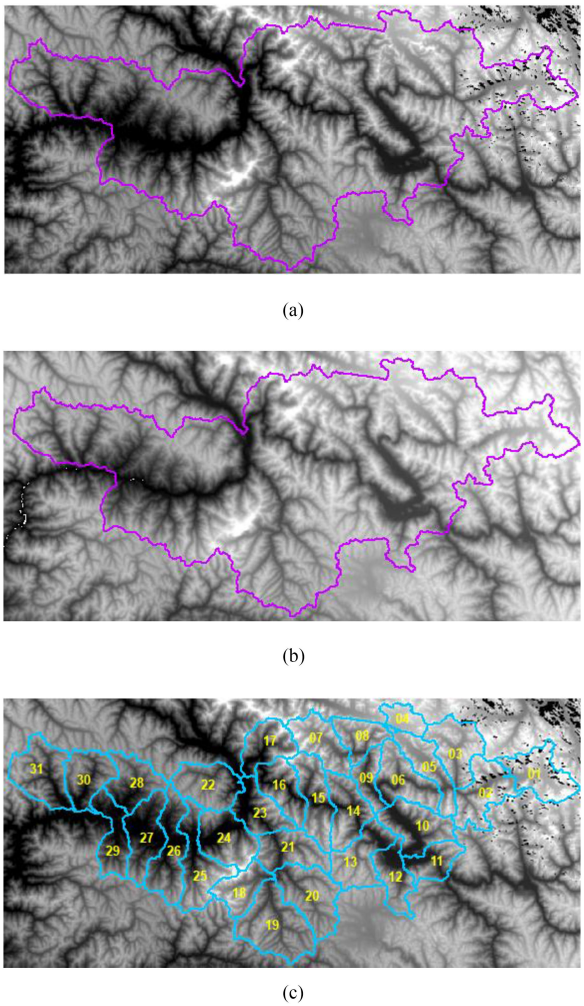

Fig. 1. DEMs of the Lower Indus subbasin. (a) SRTM DEM (11 135 columns × 5162 rows, minimum and maximum elevations, respectively, are 716 and 8583 m). (b) Cartosat DEM (11 130 columns × 5173 rows, minimum and maximum elevations, respectively, are 663 and 7640 m). (c) 31 watersheds within the lower Indus subbasin.

DEM analysis and surficial characterization. Classification of watersheds based on surface roughness indexes that vary from direction to direction is addressed here. It is hypothesized that the classification based on directional roughness of the watersheds would be a first step to relate the distinct surficial phenomena with watershed-wise geophysical processes, and also with the dominant flow direction within the watersheds.

Grayscale morphological interpolation and the use of morphological distances have shown promising results in morphing the source DEM into the target DEM [55], and in pairing the hierarchically partitioned DEMs [32]. Grayscale granulometric analysis, a technique of mathematical morphology [57]–[59]—that yielded promising results in the context of processing and analysis of remotely sensed satellite data [34]–[44]—is applied for classification of the watersheds derived from DEMs. In particular, grayscale directional granulometric analysis is applied for classification of 31 watersheds derived from SRTM and Cartosat DEMs of the Lower Indus subbasin [see Fig. 1(a)–(c)]. The Indus basin extends over China (Tibet), India, Afghanistan,

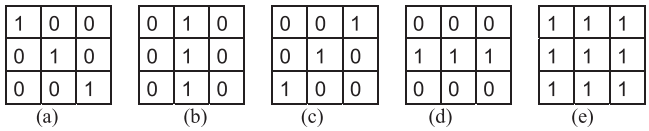

Fig. 2. Directional structuring elements (a) B^1, (b) B^2, (c) B^3, (d) B^4, and compact structuring element (e) B.

and Pakistan draining an area of 1 165 500 km^2. In India, the basin spreads over an area of 321 289 km^2, which is nearly 9.8% of the total geographical area. The Indus basin is subdivided into 14 subbasins. The geographical extent of the study area viz. Lower Indus subbasin lies between 73° 11′ to 76° 44′ East Longitudes and 34° 42′ to 36° 9′ North Latitudes. Lower Indus subbasin has a total catchment area of 23 894 km^2 and is divided into 31 watersheds with size ranging from 319 to 1270 km^2.

The characterization of terrestrial surfaces via fractal dimensions [1]–[10] has no option to compute the direction-specific roughness. In this article, we show how SRTM and Cartosat DEMs (both with spatial resolution of 30 m) and the basins and corresponding watersheds decomposed from them have been employed in directional granulometry based classification of watersheds in order to automatically determine: 1) the direction in which the watershed is vulnerable to perturbation, and 2) the orientation of the watershed.

This article is organized as follows. Section II summarizes the basic grayscale morphological transformations. Methodology and its demonstration on a geophysical subbasin are given in Section III. Section IV provides experimental results obtained for 31 watersheds represented by SRTM and Cartosat DEMs, and concluding remarks are given in Section V.

II. Grayscale Morphological Transformations

Nonlinear grayscale mathematical morphological transformations such as dilation, erosion, opening, and closing [58] are important in processing and analysis of grayscale, multispectral, and hyperspectral images. They are immensely useful in all areas of spatial data sciences [15], [52]. We restrict this section to explain only essential grayscale morphological transformations that include dilation (1), erosion (2), opening (3), and their multiscale versions (4)–(6).

Let f be a raster image depicting elevation values in a grayscale form across the spatial coordinates (x, y). Let B [see Fig. 2(e)] be a structuring element with certain characteristic information employed to probe $f(x, y)$ to retrieve morphological descriptors.

A. Grayscale Dilation, Erosion, and Opening

The dilation (erosion) of f by flat structuring element B replaces the value of f at a pixel (x, y) by the *maxima* (*minima*) of the values of f over a structuring element B [16], [17]. Morphological grayscale dilation and erosion of f with respect to B are defined as (1) and (2), respectively

$$f \oplus B = \max_{i,j \in B} \{f(x+i), (y+j)\} \tag{1}$$

$$f \ominus B = \min_{i,j \in B} \{f(x+i), (y+j)\}. \tag{2}$$

Morphological opening transformation, which is an idempotent transformation, involves morphological erosion followed by dilation of *f* by *B* as follows:

$$f \circ B = (f \ominus B) \oplus B \tag{3}$$

where o is the symbol for morphologic opening. We shall denote the dilation, the erosion, and the opening of *f* by *B*, respectively, by$(f \oplus B)$, $(f \ominus B)$, and$(f \circ B)$.

B. Multiscale Morphological Transformations

Multiscale morphological transformations (4)–(6) can be performed by varying the size of the *structuring element nB*, where $n = 0, 1, 2, \ldots, N$. Dilation, erosion, and opening can also be performed iteratively as follows:

$$f \oplus nB = (f \oplus B) \oplus B \oplus \cdots \oplus B \tag{4}$$

$$f \ominus nB = (f \ominus B) \ominus B \ominus \cdots \ominus B \tag{5}$$

$$f \circ nB = (f \ominus B) \ominus B \ominus \cdots \ominus B \oplus B \oplus B \oplus \cdots \oplus B. \tag{6}$$

The primitive structuring elements are shown in Fig. 2(a)–(e); note that all the structuring elements are symmetric about the origins that are chosen at the center. The sizes of structuring elements would be increased by dilating the primitive *B* with itself to get the size increased to 2*B*, and 2*B* would be dilated with *B* to get 3*B*, and *n*th size *B* is typically achieved by $B \oplus B \oplus \cdots \oplus B$ for *n* times. The reader is referred to [57]–[59] for a more detailed exposition of these fundamental transformations and their algebraic properties.

C. Directional Structuring Elements

Structuring element (*B*) of primitive size 3×3 with nine elements, square in shape, and symmetric about the origin [see Fig. 2(e)], and four directional structuring elements [see Fig. 2(a)–(d)] that could be decomposed from Fig. 2(e) are considered to compute a host of basic parameters.

These directional structuring elements, respectively, denoted as B^1, B^2, B^3, and B^4 represent NW–SE, N–S, NE–SW, and E–W directions; they are symmetric about origin and satisfy the following properties.

1) $B^1 \cup B^2 \cup B^3 \cup B^4 = B$.
2) $f \oplus (B^1 \cup B^2 \cup B^3 \cup B^4) = f \oplus B$.
3) $f \ominus (B^1 \cup B^2 \cup B^3 \cup B^4) = f \ominus B$.
4) $f \circ (B^1 \cup B^2 \cup B^3 \cup B^4) = f \circ B$.
5) $B^i \oplus B^i \oplus B^i \oplus \cdots \oplus B^i = nB^i = \bigcup_{i=1}^{4} nB^i = nB$.
6) $f \ominus \bigcup_{i=1}^{4} nB^i = f \ominus nB$.
7) $f \oplus \bigcup_{i=1}^{4} nB^i = f \oplus nB$.
8) $f \circ \bigcup_{i=1}^{4} nB^i = f \circ nB$.

III. Granulometries in Watershed Roughness

Granulometric indexes and shape–size complexity measures quantify the surficial roughness [49], [50]. In what follows in this section includes computations of global and directional granulometric index values of subbasin (*f*), watersheds (f^k) of *f*, as well as high- and low-directional granulometric indexes.

A. Granulometry

Recursive application of grayscale morphological opening of a function (subbasin) *f* by sequentially changing the size of structuring element *B*, without changing other characteristic information such as the shape, orientation, and symmetry, leads to grayscale granulometric analysis. Principle of granulometries [57], [58] is the main idea involved in automatic classification of basins and watersheds. Such granulometric analysis of *f(x,y)* with respect to *B* involves the following sequential steps:

1) iterative multiscale grayscale morphological opening of *f(x,y)*, $f \circ nB$, where $n = 0, 1, 2, \ldots, N$;
2) computation of pattern spectra PS(*f*/*B*) as the areal difference between $f \circ nB$ and $f \circ (n+1)B$;
3) computation of granulometric index of *f(x,y)* with respect to *B*, *H(f/B)*.

Granulometric index would be computed for subbasin (*f*), and watersheds (f^k) partitioned from DEMs according to (7). Under the increasing cycles of opening (foreground granulometries), the area under the function gets diminished, and the loss of information under two successive cycles of opening is termed by the pattern spectrum at the particular order

$$H(f/B) = -\sum_{n=0}^{N} p_n \ln p_n \tag{7}$$

where

$$p_n = \frac{A(f \circ nB) - A(f \circ (n+1)B)}{A(f)}, n = 0, 1, 2, \ldots N \tag{8}$$

where $A(f) = \sum_{x,y} f(x,y)$ is the area of the 2-D function.

The quantitative characterization of basin surfaces partitioned from DEMs via directional structuring elements is important, as direction-specific roughness values provide us with:

1) general flow direction and orientation of the basins;
2) direction-specific vulnerability under the perturbations in that direction;
3) intrarelationships among the watersheds of a basin.

B. Directional Granulometry

Instead of choosing a structuring element (*B*) that is a circle in eight connected grids, four directional structuring elements (B^i), where $i = 1, 2, 3, 4$, that are symmetric about the origins would be considered to compute p_n and $H(f/B^i)$. In turn, (7) and (8) would take the form of (9) and (10)

$$H\left(f/B^i\right) = -\sum_{n=0}^{N} p_n \ln p_n \tag{9}$$

where

$$p_n = \frac{A\left(f \circ nB^i\right) - A\left(f \circ (n+1)B^i\right)}{A(f)} \tag{10}$$

where n and i denote size of the structuring element and index of the directional structuring element, respectively. The computations of global and directional granulometric index values of subbasin (*f*) denoted as *H(f/B)* and *H(f/B^i)* could be extended

TABLE I
GRAYSCALE GRANULOMETRIES

SEs /	SRTM DEM				Cartosat DEM			
Cycles	*100*	*200*	*1000*	*5000*	*100*	*200*	*1000*	*5000*
B^1	0.68	1.11	1.67	2.57	0.65	1.11	1.77	2.76
B^2	0.50	0.89	1.83	2.40	0.44	0.83	1.84	2.83
B^3	0.70	1.22	2.17	2.76	0.47	0.73	1.26	2.29
B^4	0.54	0.94	1.97	2.57	0.53	0.97	2.06	2.29
B	1.02	1.57	2.44	2.68	0.87	1.48	2.53	2.16

to the watersheds (f^k). The notations for watershed level are $H(f^k/B)$ and $H(f^k/B^i)$.

C. High- and Low-Directional Granulometric Index

Besides watershed-specific global granulometric index values (11), high (low) directional granulometric index values, HDGI(f^k) and LDGI(f^k), could be derived for each watershed from its corresponding four directional granulometric index values, $H(f^k/B^i)$, according to (12) and (13)

$$\mathrm{GI}\left(f^k/B\right) = H\left(f^k/B\right) \tag{11}$$

$$\mathrm{HDGI}\left(f^k/B^i\right) = \max_{\forall i}\left(H\left(f^k/B^i\right)\right) \tag{12}$$

$$\mathrm{LDGI}\left(f^k/B^i\right) = \min_{\forall i}\left(H\left(f^k/B^i\right)\right). \tag{13}$$

Granulometric index of f^k is B^i dependent. We adopted the global and directional granulometric index values of subbasin and the corresponding watersheds for automatic classification of watersheds into several classes.

D. Automatic Detection of Watershed Orientation

The direction in which the watershed yields highest granulometric index is the orientation of the watershed. Out of four directional structuring elements employed here, if the watershed under transformation yields 4, 3, 2, and 1 granulometric index values, respectively, with respect to B^1, B^2, B^3, and B^4, then the orientation of the watershed is from north-west to south-east.

E. Model Demonstration

According to (7)–(10), granulometric indexes were computed for the Lower Indus subbasin and its 31 watersheds derived from DEM data. Multiscale morphological openings were performed on SRTM and Cartosat DEMs of the Lower Indus subbasin to derive granulometric indexes (see Table I) with respect to the compact structuring element B [see Fig. 2(e)], and the four directional structuring elements [see Fig. 2(a)–(d)]. Mathematical morphology operations were performed using the tools available in MATLAB and for surface volume estimations, ArcGIS software was used.

SRTM DEM of the Lower Indus subbasin [see Fig. 1(a)] under the influence of grayscale opening cycles of 10, 100, 1000, and 5000 with respect to B is shown in Fig. 3(a)–(d). With increasing cycles of opening the DEM loses information, in other words the area, as shown in Fig. 3(a)–(d). The DEM under the influence of 100 cycles of opening by four directional structuring

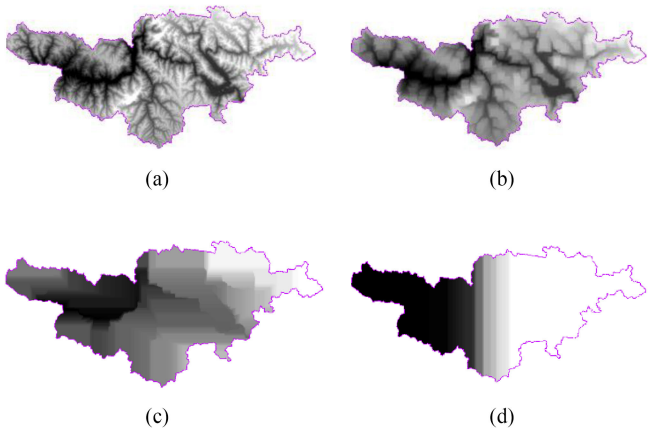

Fig. 3. Lower Indus basin shown in Fig. 1(a) after multiscale opening by (a) 10, (b) 100, (c) 1000, and (d) 5000 cycles.

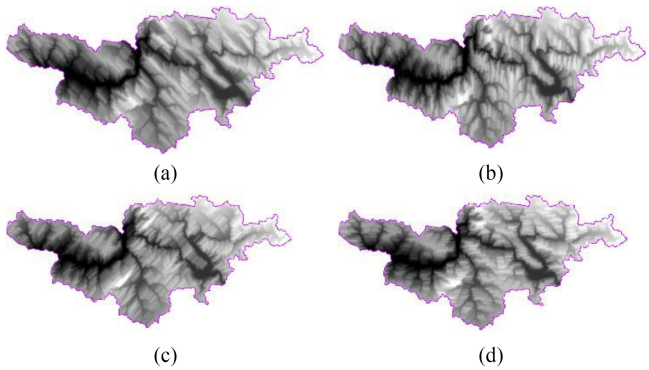

Fig. 4. Lower Indus subbasin subject to multiscale openings by (a) B^1, (b) B^2, (c) B^3, and (d) B^4 after 100 cycles.

elements is shown in Fig. 4(a)–(d). Global granulometric indexes computed for the Lower Indus subbasin DEM (both SRTM and Cartosat) with respect to compact and symmetric flat B are 2.68 and 2.16, respectively (see Table I). Further similar granulometric analysis is performed on each of the watersheds derived from SRTM and Cartosat DEMs f^k with respect to four directional structuring elements. The pattern spectra values of all 31 watersheds computed are shown as a function of B and four directional structuring elements (B^i) [see Fig. 5(a) and (b)].

For every f^k, granulometric index was calculated according to (7)–(10) with respect to each directional structuring element. Watersheds representing in grayscale forms of this region [see Fig. 1(c)] are subjected to grayscale granulometric analysis with respect to one compact structuring element [see Fig. 2(e)] and four directional structuring elements—B^1, B^2, B^3, and B^4 [see Fig. 2(a)–(d)]. Table II depicts granulometric indexes of 31 watersheds of the Lower Indus subbasin derived from SRTM DEM (values in parentheses are derived from Cartosat DEM). The higher the index value, the higher is the roughness with respect to that specific B^i. There would be n number of granulometric index values for a spatial field that is subjected to grayscale granulometries with respect to n distinct structuring elements.

Selected snapshots of f^{19} subject to multiscale openings by B, B^1, B^2, B^3, and B^4 at cycles 0, 200, 400, 600, 800, and 1000

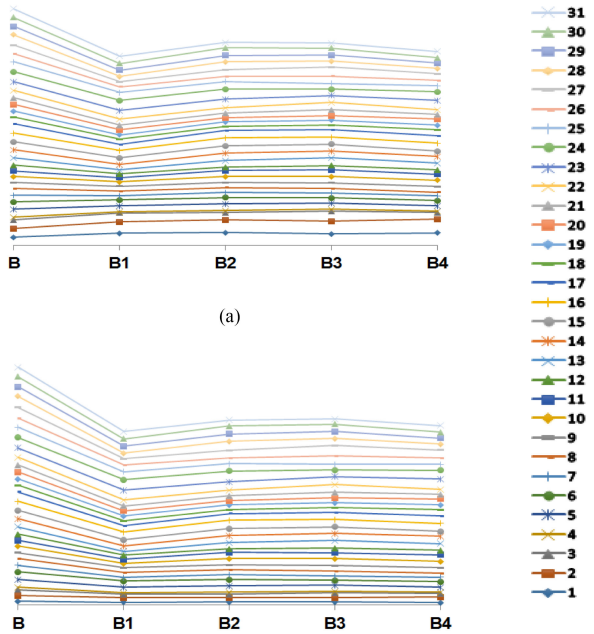

(a)

(b)

Fig. 5. Pattern spectra values of 31 watersheds of the Lower Indus subbasin plotted as functions of B, B^1, B^2, B^3, and B^4 till converging cycles. (a) SRTM DEM. (b) Cartosat DEM.

TABLE II
GRANULOMETRIC INDEXES OF 31 WATERSHEDS

WS No.	B1	B2	B3	B4	B
1	3.984 (1.029)	4.158 (1.116)	3.686 (1.284)	4.034 (1.004)	2.584 (1.454)
2	3.629 (1.766)	4.004 (1.836)	4.169 (1.615)	4.347 (2.073)	2.874 (2.296)
3	2.883 (1.464)	2.456 (1.378)	3.125 (1.804)	2.154 (1.356)	2.735 (2.282)
4	0.403 (0.450)	0.618 (0.670)	0.773 (0.730)	0.498 (0.565)	0.885 (1.011)
5	1.918 (2.305)	2.133 (2.475)	1.936 (2.301)	1.649 (1.949)	2.589 (3.106)
6	1.926 (2.398)	2.107 (2.563)	1.680 (2.127)	1.883 (2.357)	2.351 (2.948)
7	1.288 (1.541)	1.617 (1.941)	1.423 (1.697)	1.447 (1.734)	2.182 (2.665)
8	1.487 (1.779)	1.597 (1.934)	1.540 (1.895)	1.164 (1.432)	2.172 (2.645)
9	1.601 (1.991)	1.668 (2.044)	1.847 (2.264)	1.820 (2.249)	1.883 (2.348)
10	1.468 (1.831)	1.895 (2.431)	2.069 (2.665)	2.068 (2.677)	2.011 (2.594)
11	1.304 (1.655)	1.960 (2.526)	2.054 (2.383)	1.932 (2.527)	1.814 (2.350)
12	1.271 (1.609)	1.114 (1.391)	1.468 (1.878)	1.348 (1.731)	1.799 (2.300)
13	1.182 (1.479)	2.011 (2.409)	2.470 (3.007)	2.165 (2.697)	2.400 (3.016)
14	1.754 (2.089)	2.449 (2.855)	2.189 (2.666)	2.246 (2.843)	2.5 00 (3.157)
15	2.084 (2.529)	2.344 (2.800)	2.222 (2.704)	1.591 (1.954)	2.701 (3.371)
16	2.493 (3.128)	2.663 (3.218)	2.328 (2.828)	2.638 (3.242)	2.693 (3.522)
17	1.853 (2.335)	2.275 (2.706)	2.309 (2.919)	2.300 (2.894)	3.067 (3.824)
18	1.677 (2.056)	1.274 (1.579)	1.515 (1.870)	2.015 (2.496)	2.108 (2.674)
19	1.471 (1.863)	1.570 (1.993)	1.624 (2.061)	1.523 (1.930)	1.942 (2.483)
20	1.674 (2.103)	1.285 (1.613)	1.429 (1.794)	1.926 (2.421)	2.163 (2.785)
21	1.529 (1.931)	1.478 (1.876)	1.844 (2.318)	1.491 (1.884)	2.157 (2.749)
22	1.830 (2.328)	1.809 (2.257)	2.403 (3.087)	1.450 (1.810)	2.328 (2.979)
23	2.883 (3.951)	2.663 (3.318)	2.271 (3.130)	3.038 (4.139)	2.884 (3.848)
24	3.108 (4.047)	3.314 (4.291)	2.052 (2.609)	2.794 (3.561)	3.148 (4.127)
25	2.579 (3.300)	2.458 (2.956)	1.817 (2.332)	1.951 (2.446)	3.223 (4.079)
26	1.889 (2.552)	1.615 (2.181)	2.361 (3.209)	1.710 (2.331)	2.626 (3.562)
27	1.706 (2.551)	2.085 (3.112)	2.856 (4.243)	2.178 (3.262)	2.892 (4.313)
28	1.679 (2.234)	2.667 (3.553)	2.016 (2.684)	1.763 (2.344)	3.279 (4.472)
29	2.032 (2.897)	2.038 (2.928)	2.008 (2.873)	1.641 (2.377)	2.617 (3.798)
30	2.127 (2.795)	2.381 (3.143)	2.166 (2.851)	1.784 (2.349)	2.976 (3.955)
31	2.375 (3.036)	1.856 (2.389)	1.664 (2.140)	2.053 (2.650)	2.821 (3.661)

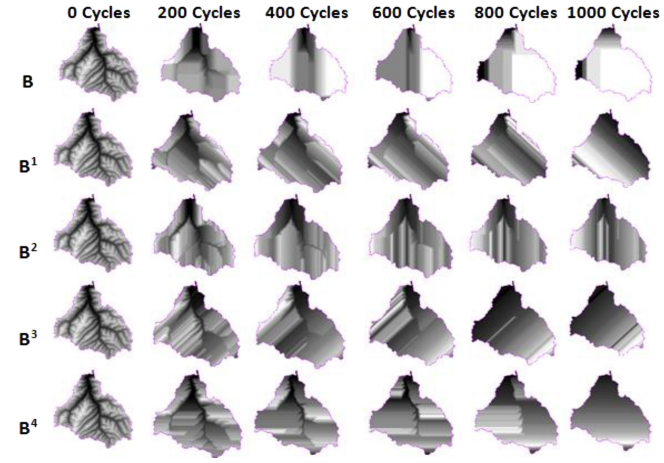

Fig. 6. Evolution of watershed 19 under recursive opening cycles with respect to B, B^1, B^2, B^3, and B^4.

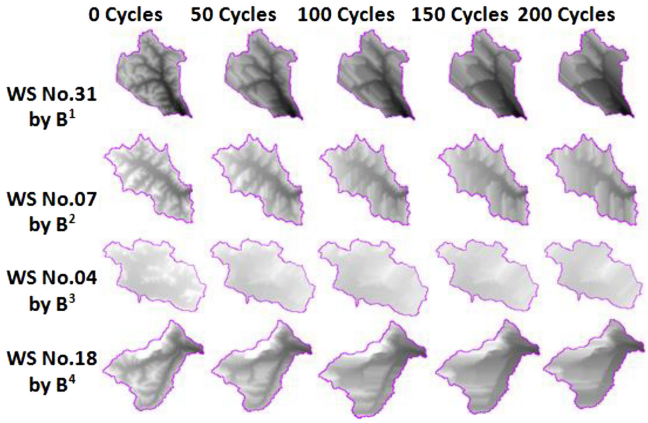

Fig. 7. Behavior of watersheds from Cartosat DEM under multiscale opening of (a) f^{31} by B^1, (b) f^7 by B^2, (c) f^4 by B^3, and (d) f^{18} by B^4, at the cycles 0, 50, 100, 150, and 200.

are shown in Fig. 6. Watershed 19 [see Fig. 1(b)] was subjected to various higher cycles of opening, for instance, cycles of 0, 200, 400, 600, 800, and 1000, respectively, with respect to B [where B is the structuring element shown in Fig. 2(e)]. The first row of Fig. 6 depicts the result.

For better understanding, the evolution of four watersheds under the influence of multiscale opening, with respect to the structuring elements that have yielded higher roughness, is shown in Fig. 7. The figure shows that the pattern behaviors of f^ks yielded higher granulometric indexes in different directions.

IV. WATERSHEDS CLASSIFICATION: RESULTS AND ANALYSIS

In earlier studies, surficial roughness values had been computed via granulometries with respect to a compact symmetric flat structuring element and also via fractal dimensions. None of the earlier studies has provided directional roughness values. For the first time, in this study the directional roughness values have been computed via granulometries with respect to four directional structuring elements. Furthermore, the watersheds decomposed from the basin are categorized based on the high- and low-directional granulometric values. We hope that this

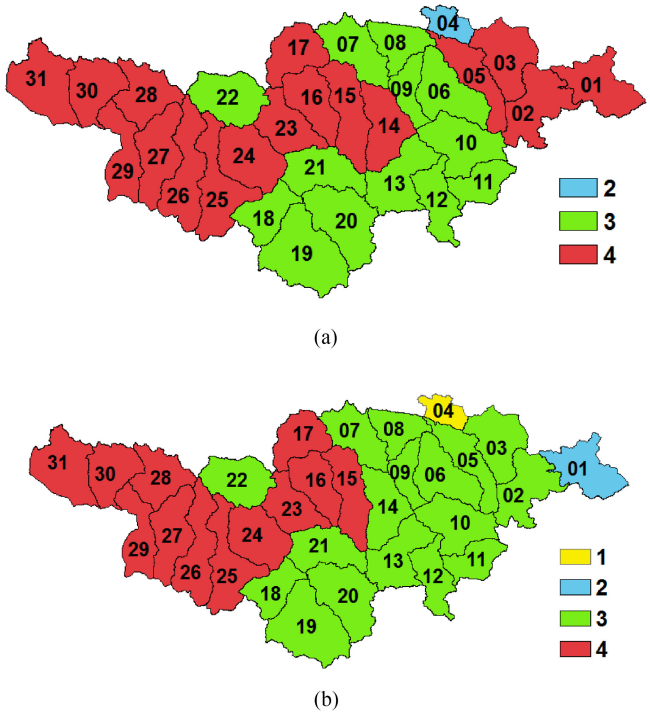

Fig. 8. Normalized granulometric indexes. (a) SRTM DEM. (b) Cartosat DEM. Categories: 1) 0–0.25, 2) 0.26–5.0, 3) 0.51–0.75, and 4) 0.76–1.0.

study would provide insights to geoscience and remote sensing researchers. For automatic classification of watersheds represented as grayscale DEMs according to directional granulometric analysis, we considered a subbasin [see Fig. 1(a) and (b)] and its corresponding 31 watersheds denoted with f^1, f^2,…,f^{31} [see Fig. 1(c)]. Application of directional granulometries, as explained in the previous section, is extended for automatic classification of watersheds derived from SRTM and Cartosat DEMs [see Fig. 1(a) and (b)]. The granulometric index values computed with respect to four B^is for each watershed are given in Table II. The granulometric indexes obtained are grouped into four categories by normalization. Fig. 8 shows the maps generated based on the classification of watersheds via granulometric index values computed with respect to B according to (11).

It is observed that the watersheds with orientation similar to $\boldsymbol{B^i}$**s** yield higher directional granulometric indexes (see Table II). From Table II, it is also seen that the watersheds 25 and 31 are rough in the direction of NW–SE ($\boldsymbol{B^1}$). Watersheds 2, 18, 20, and 23 are rough in direction similar to the $\boldsymbol{B^4}$. The direction of the structuring element for which the resulting granulometric index is highest (lowest) among the four directional possibilities for each of the 31 watersheds is the direction of highest (lowest) roughness. Maps generated based on the classification of watersheds with respect to high- and low-directional granulometric indexes computed according to (12) and (13) are shown in Figs. 9 and 10, respectively. Fig. 9(a) and (b), respectively, shows the 31 watersheds derived from SRTM and Cartosat DEMs categorized with respect to high-directional granulometric index values. Fig. 10(a) and (b) shows the classification with respect to low-directional granulometric index values.

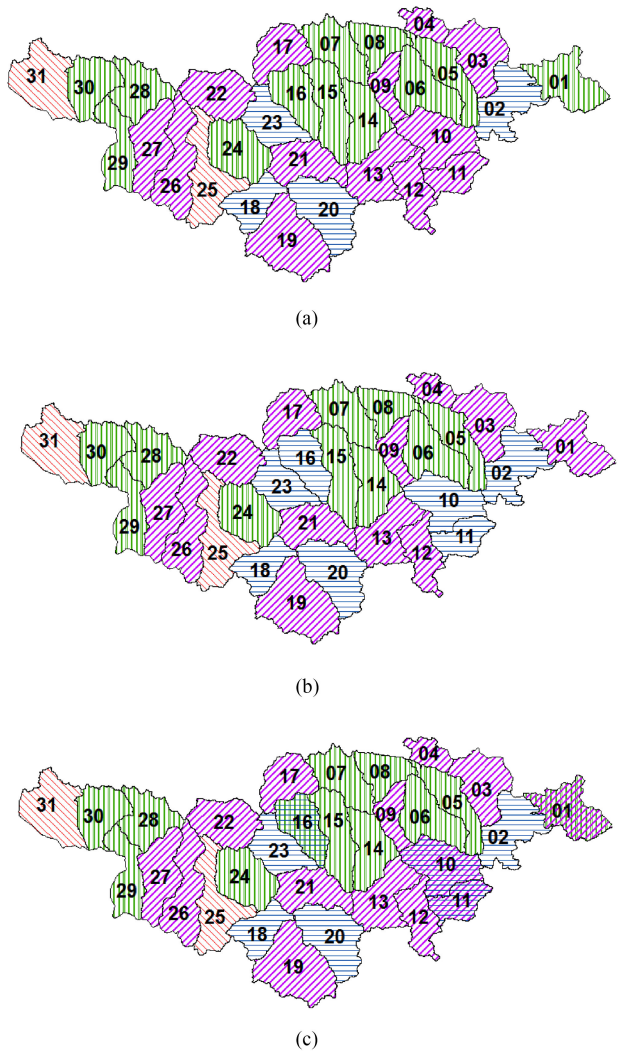

Fig. 9. High-directional granulometric index values of 31 watersheds derived from (a) SRTM DEM, (b) Cartosat DEM, and (c) variations in results across SRTM and Cartosat DEMs (cross wired symbols).

It is observed from Figs. 9 and 10 that the classification results shown for 31 watersheds derived from SRTM and Cartosat DEMs are significantly similar. Classification of geophysical basins and watersheds with respect to various surficial roughness parameters computed via directional grayscale granulometric analysis is shown in this article. Studying the behavior of spatial fields like DEMs via directional grayscale granulometries provides a solution for automatic classification of watersheds, and is superior to those methods that involve approximations. This classification approach is stable due to the fact that 1) every pixel of each spatial field would be involved in the process of multiscale opening, and 2) shape–size content of the field is investigated with respect to B^i. Spatial fields such as DEMs that are in raster format are better inputs for developing spatio–temporal models to explain the dynamical behavior of phenomena and processes.

The present study only considered SRTM and Cartosat DEMs of 30-m spatial resolutions per pixel, which were generated using two different methods. However, we plan to implement

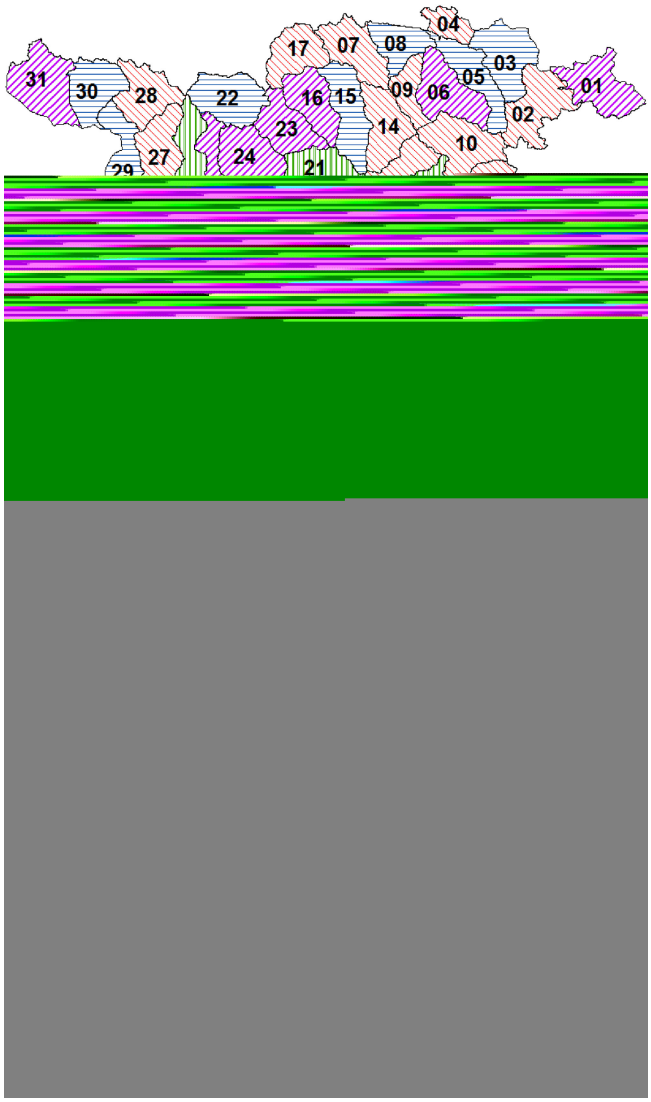

Fig. 10. Low-directional granulometric index values of 31 watersheds derived from (a) SRTM DEM, (b) Cartosat-1 DEM, and (c) variations in results across SRTM and Cartosat-1 DEMs (cross wired symbols).

a similar approach to see variations in the granulometric index values (with respect to B, B^1–B^4) of basins with the change of spatial resolutions of DEM data. The numbers of directions that are now considered are four (NW–SE, N–S, NE–SW, E–W). The number of directions could be increased to eight by taking the bipoint structuring elements as NW, N, NE, W, SE, S, SW, and E. However, these structuring elements are asymmetric about the origin, and while performing multiscale opening based granulometries, one needs to make sure that the structuring element is transposed during the dilation process. It would be interesting to adopt the line (directional) structuring elements, in an interpolated way to get a large number of directional options [60]–[62] instead of four directions considered in this article, and to compute a large number directional granulometric indexes that might result in more categories in the classification. Furthermore, a most interesting and worthwhile study is to apply the approach proposed in this article on global elevation model such as NASADEM and the ASTER GDEM [63] to classify hierarchically partitioned basins and watersheds with respect to both global and directional granulometric index values.

V. Conclusion

An approach based on directional grayscale granulometries is provided for classification of watersheds derived from both SRTM and Cartosat-1 DEMs. We hypothesize that the watersheds with high granulometric index in the B^i direction are the watersheds weak in that direction, and are prone to have higher capacity to change under perturbations. In all, 31 watersheds derived from both SRTM DEM and Cartosat DEM were categorized into four categories with respect to directional granulometric values. Classification results shown for the 31 watersheds derived from both SRTM and Cartosat DEMs are significantly similar. The direction-specific classification of watersheds provides insights for domain experts to explore potential links with several parameters of significance to geophysics, seismology, geomorphology, and geology. It has also been found that the orientation of watersheds and the general flow direction within those watersheds are in the direction in which the watersheds yield high-directional granulometric index. Application of this approach on the physiographically distinct fluvial, tidal, and desert basins derived from DEMs is interesting and would provide further insights. Extending the approach demonstrated in this article on the watersheds of the Lower Indus basin to the DEM of whole earth and earth-like planetary surfaces for the classification of hierarchically partitioned geophysical basins ranging from very large basins to microwatershed level would be a worthy exercise for domain experts to explore the links between surficial processes and subsurface processes.

Acknowledgment

The authors are most grateful to the two anonymous reviewers and the Associate Editor for their useful comments and suggestions, which have led to significant improvements both in content and quality on the manuscript. They also gratefully acknowledge the encouragement given by the Editor-in-Chief, Prof. J. Du, who expertly handled the earlier versions of this article. The authors are also grateful to Prof. G. Korvin for providing constructive suggestions.

References

[1] B. Mandelbrot, "Stochastic models for the earth's relief, the shape and the fractal dimension of coastlines, and the number-area rule for islands," *Proc. Nat. Acad. Sci. USA*, vol. 72, pp. 3825–3828, 1975.
[2] P. A. Burrough, "Fractal dimensions of landscapes and other environmental data," *Nature*, vol. 294, pp. 240–242, 1981.
[3] A. Woronow, "Morphometric consistency with the Hausdorff-Besicovitch dimension," *Math. Geol.*, vol. 13, pp. 201–216, 1981.
[4] B. Mandelbrot, D. Passoja, and A. Paullay, "Fractal character of fracture surfaces of metals," *Nature*, vol. 308, pp. 721–722, 1984.
[5] A. Pentland, "Fractal-based description of natural scenes," *IEEE Trans. Pattern Anal. Mach. Intell.*, vol. PAMI-6, no. 6, pp. 661–674, Nov. 1984.
[6] S. Peleg, "Multiple resolution texture analysis and classification," *IEEE Trans. Pattern Anal. Mach. Intell.*, vol. PAMI-6, no. 4, pp. 518–523, Jul. 1984.
[7] M. F. Goodchild and D. M. Mark, "The fractal nature of geographic phenomena," *Ann. Amer. Assoc. Geographers*, vol. 77, pp. 265–278, 1987.

[8] N. Dodd, "Multispectral texture synthesis using fractal concepts," *IEEE Trans. Pattern Anal. Mach. Intell.*, vol. PAMI-9, no. 5, pp. 703–707, Sep. 1987.

[9] B. Klinkenberg and K. Clarke, "Exploring the fractal mountains," in *Automated Pattern Analysis in Petroleum Exploration*, I. Palaz and S. Sengupta, Eds., New York, NY, USA: Springer-Verlag, 1992, pp. 201–212.

[10] B. Klinkenberg and M. F. Goodchild, "The fractal properties of topography: A comparison of methods," *Earth Surf. Processes Landforms*, vol. 17, pp. 217–234, 1992.

[11] I. V. Florinsky, "Derivation of topographic variables from a digital elevation model given by a spheroidal trapezoidal grid," *Int. J. Geogr. Inf. Sci.*, vol. 12, no. 8, pp. 829–852, 1998.

[12] G. E. Tucker, F. Catani, A. Rinaldo, and R. L. Bras, "Statistical analysis of drainage density from digital terrain data," *Geomorphology*, vol. 36, no. 3/4, pp. 187–202, 2001.

[13] B. S. D. Sagar and T. L. Tien, "Allometric power-law relationships in a Hortonian fractal DEM," *Geophys. Res. Lett.*, vol. 31, no. 6, 2004, Art. no. L06501.

[14] H. Mitasova, R. S. Harmon, K. J. Weaver, N. J. Lyons, and M. F. Overton, "Scientific visualization of landscapes and landforms," *Geomorphology*, vol. 137, pp. 122–137, 2012.

[15] B. S. D. Sagar, *Mathematical Morphology in Geomorphology and GISci*. Boca Raton, FL, USA, CRC Press, 2013, p. 516.

[16] C. M. Tseng, C. W. Lin, C. P. Stark, J. K. Liu, L. Y. Fei, and Y. C. Hsieh, "Application of a multi-temporal, LiDAR-derived, digital terrain model in a landslide-volume estimation," *Earth Surf. Processes Landforms*, vol. 38, no. 13, pp. 1587–1601, 2013.

[17] C. Bandaragoda *et al.*, "Enabling collaborative numerical modeling in earth sciences using knowledge infrastructure," *Environ. Model. Softw.*, vol. 120, 2019, Art. no. 104424, doi: 10.1016/j.envsoft.2019.03.020.

[18] SRTM. [Online]. Available: https://dwtkns.com/srtm30m/

[19] Cartosat-1 DEM. [Online]. Available: https://data.gov.in/resources/cartosat-1dem-version-1

[20] D. Marks, J. Dozier, and J. Frew, "Automated basin delineation from digital elevation data," *Geo-Process.*, vol. 2, pp. 299–311, 1984.

[21] J. F. O'Callaghan and D. M. Mark, "The extraction of drainage networks from digital elevation data," *Comput. Vision, Graph. Image Process.*, vol. 28, pp. 328–344, 1984.

[22] L. E. Band, "Topographic partition of watersheds with digital elevation models," *Water Resour. Res.*, vol. 22, no. 1, pp. l5–24, 1986.

[23] D. G. Tarboton, R. L. Bras, and I. Rodriguez-Iturbe, "On the extraction of channel networks from digital elevation data," *Hydrol. Processes*, vol. 5, no. 1, pp. 81–100, 1991.

[24] P. Soille and M. M. Ansoult, "Automated basin delineation from digital elevation models using mathematical morphology," *Signal Process.*, vol. 20, pp. 171–182, 1990.

[25] L. Vincent and P. Soille, "Watersheds in digital spaces: An efficient algorithm based on immersion simulations," *IEEE Trans. Pattern Anal. Mach. Intell.*, vol. 13, no. 6, pp. 583–598, Jun. 1991.

[26] D. G. Tarboton, "A new method for the determination of flow directions and contributing areas in grid digital elevation models," *Water Resour. Res.*, vol. 33, no. 2, pp. 309–319, 1997.

[27] G. C. Miliaresis and D. P. Argialas, "Segmentation of physiographic features from global digital elevation model/GTOPO30," *Comput. Geosci.*, vol. 25, pp. 715–728, 1999.

[28] B. S. D. Sagar, M. Venu, and D. Srinivas, "Morphological operators to extract channel networks from digital elevation models," *Int. J. Remote Sens.*, vol. 21, no. 1, pp. 21–30, 2000.

[29] B. S. D. Sagar, M. B. R. Murthy, C. Babu Rao, and B. Raj, "Morphological approach to extract ridge-valley connectivity networks from digital elevation models (DEMs)," *Int. J. Remote Sens.*, vol. 24, no. 3, pp. 573–581, 2003.

[30] L. Chockalingam and B. S. D. Sagar, "Automatic generation of subwatershed map from digital elevation model: A morphological approach," *Int. J. Pattern Recognit. Artif. Intell.*, vol. 17, no. 2. pp. 269–274, 2003.

[31] D. Sathymoorthy, P. Radhakrishnan, and B. S. D. Sagar, "Morphological segmentation of physiographic features from DEM," *Int. J. Remote Sens.*, vol. 28, no. 15, pp. 3379–3394, 2007.

[32] B. S. D. Sagar and S. L. Lim, "Ranks for pairs of spatial fields via metric based on grayscale morphological distances," *IEEE Trans. Image Process.*, vol. 24, no. 3, pp. 908–918, Mar. 2015.

[33] C. A. Rishikeshan and H. Ramesh, "An automated mathematical morphology driven algorithm for water body extraction from remotely sensed images," *ISPRS J. Photogramm. Remote Sens.*, vol. 146, pp. 11–21, 2018.

[34] J. A. Benediktsson, M. Pesaresi, and K. Arnason, "Classification and feature extraction for remote sensing images from urban areas based on morphological transformations," *IEEE Trans. Geosci. Remote Sens.*, vol. 41, no. 9, pp. 1940–1949, Sep. 2003.

[35] J. A. Benediktsson, J. A. Palmason, and J. Sveinsson, "Classification of hyperspectral data from urban areas based on extended morphological profiles," *IEEE Trans. Geosci. Remote Sens.*, vol. 43, no. 3, pp. 480–491, Mar. 2005.

[36] T. Barata and P. Pina, "A morphological approach for feature space partitioning," *IEEE Geosci. Remote Sens. Lett.*, vol. 3, no. 1, pp. 173–177, Jan. 2006.

[37] M. Dalla Mura, J. A. Benediktsson, F. Bovolo, and L. Bruzzone, "An unsupervised technique based on morphological filters for change detection in very high resolution images," *IEEE Geosci. Remote Sens. Lett.*, vol. 5, no. 3, pp. 433–437, Jul. 2008.

[38] X. Huang, L. P. Zhang, and L. Wang, "Evaluation of morphological texture features for mangrove forest mapping and species discrimination using multispectral IKONOS imagery," *IEEE Geosci. Remote Sens. Lett.*, vol. 6, no. 3, pp. 393–397, Jul. 2009.

[39] M. Dalla Mura, J. A. Benediktsson, B. Waske, and L. Bruzzone, "Morphological attribute profiles for the analysis of very high resolution images," *IEEE Trans. Geosci. Remote Sens.*, vol. 48, no. 10, pp. 3747–3762, Oct. 2010.

[40] M. Dalla Mura, A. Villa, J. A. Benediktsson, J. Chanussot, and L. Bruzzone, "Classification of hyperspectral images by using extended morphological attribute profiles and independent component analysis," *IEEE Geosci. Remote Sens. Lett.*, vol. 8, no. 3, pp. 542–546, May 2011.

[41] M. Dalla Mura, "Advanced techniques based on mathematical morphology for the analysis of remote sensing images," Doctoral dissertation, Dept. Inf. Eng. Comput. Sci., University of Trento, Trento, Italy, 2011.

[42] M. Pedergnana, P. R. Marpu, M. Dalla Mura, J. A. Benediktsson, and L. Bruzzone, "Classification of remote sensing optical and LiDAR data using extended attribute profiles," *IEEE J. Sel. Topics Signal Process*, vol. 6, no. 7, pp. 856–865, Nov. 2012.

[43] P. Wang, M. Dalla Mura, J. Chanussot, and G. Zhang, "Soft-then-hard super-resolution mapping based on pansharpening technique for remote sensing image," *IEEE J. Sel. Topics Appl. Earth Observ. Remote Sens.*, vol. 12, no. 1, pp. 334–344, Jan. 2019.

[44] S. Liu, D Marinelli, L Bruzzone, and F Bovolo, "A review of change detection in multitemporal hyperspectral images: Current techniques, applications, and challenges," *IEEE Geosci. Remote Sens. Mag.*, vol. 7, no. 2, pp. 140–158, Jun. 2019.

[45] G. C. Miliaresis and D. P. Argialas, "Quantitative representation of mountain objects extracted from the global digital elevation model (GTOPO30)," *Int. J. Remote Sens.*, vol. 23, pp. 949–964, 2002.

[46] L. T. Tay, B. S. D. Sagar, and H. T. Chuah, "Analysis of geophysical networks derived from multiscale digital elevation models: A morphological approach," *IEEE Geosci. Remote Sens. Lett.*, vol. 2, no. 4, pp. 399–403, Oct. 2005.

[47] L. T. Tay, B. S. D. Sagar, and H. T. Chuah, "Granulometric analysis of basin-wise DEMs: A comparative study," *Int. J. Remote Sens.*, vol. 28, no. 15, pp. 3363–3378, 2007.

[48] B. S. D. Sagar, N. Rajesh, S. A. Vardhan, and P. Vardhan, "Metric based on morphological dilation for the detection of spatially significant zones," *IEEE Geosci. Remote Sens. Lett.*, vol. 10, no. 3, pp. 500–504, May 2013.

[49] S. A. Vardhan, B. S. D. Sagar, N. Rajesh, and H. M. Rajashekara, "Automatic detection of orientation of mapped units via directional granulometric analysis," *IEEE Geosci. Remote Sens. Lett.*, vol. 10, no. 6, pp. 1449–1453, Nov. 2013.

[50] B. S. D. Sagar, "Variable-specific classification of zones, pairs of zones, and clusters of a spatial system via modified gravity model," *IEEE Trans. Emerg. Topics Comput.*, vol. 7, no. 2, pp. 230–241, Apr.–Jun. 2019.

[51] B. S. D. Sagar, D. Srinivas, and B. S. Parakasa Rao, "Fractal skeletal based channel networks in a triangular initiator basin," *Fractals*, vol. 9, no. 4. pp. 429–437, 2001.

[52] B. S. D. Sagar, "Visualization of spatiotemporal behavior of discrete maps via generation of recursive median elements," *IEEE Trans. Pattern Anal. Mach. Intell.*, vol. 32, no. 2, pp. 378–384, Feb. 2010.

[53] H. M. Rajashekara, P. Vardhan, and B. S. D. Sagar, "Generation of zonal map from point data via weighted skeletonization by influence zone," *IEEE Geosci. Remote Sens. Lett.*, vol. 9, no. 3, pp. 403–407, May 2012.

[54] B. S. D. Sagar, "Cartograms via mathematical morphology," *Inf. Vis.*, vol. 13, no. 1, pp. 42–58, 2014.
[55] B. S. D. Sagar and S. L. Lim, "Morphing of grayscale DEMs via morphological interpolations," *IEEE J. Sel. Topics Appl. Earth Observ. Remote Sens.*, vol. 8, no. 11, pp. 5190–5198, Nov. 2015.
[56] B. S. D. Sagar and J. Serra, "Spatial information retrieval, analysis, reasoning and modelling," *Int. J. Remote Sens.*, vol. 31, no. 22, pp. 5747–5750, 2010.
[57] G. Matheron, *Random Sets and Integral Geometry*. Hoboken, NJ, USA: Wiley, 1975.
[58] J. Serra, *Image Analysis and Mathematical Morphology*. London, U.K.: Academic, 1982.
[59] P. Maragos, "Pattern spectrum and multiscale shape representation," *IEEE Trans. Pattern Anal. Mach. Intell.*, vol. 11, no. 7, pp. 701–716, Jul. 1989.
[60] P. Soille, E. J. Breen, and R. Jones, "Recursive implementation of erosions and dilations along discrete lines at arbitrary angles," *IEEE Trans. Pattern Anal. Mach. Intell.*, vol. 18, no. 5, pp. 562–567, May 1996.
[61] P. Soille and H. Talbot, "Directional morphological filtering," *IEEE Trans. Pattern Anal. Mach. Intell.*, vol. 23, no. 11, pp. 1313–1329, Nov. 2001.
[62] C. L. Luengo Hendriks and L. J. van Vliet, "Using line segments as structuring elements for sampling-invariant measurements," *IEEE Trans. Pattern Anal. Mach. Intell.*, vol. 27, no. 11, pp. 1826–1831, Nov. 2005.
[63] R. Crippen *et al.*, "NASADEM global elevation model: Methods and progress," *Int. Arch. Photogramm., Remote Sens. Spatial Inf. Sci.*, vol. XLI-B4, pp. 125–128, 2016.

Kannan Nagajothi (M'18) received the B.Sc. degree in physics from Bharathiar University, Coimbatore, India, in 1986, and the master's degree in computer applications from Indira Gandhi National Open University, New Delhi, India, in 2002.

He is currently a Senior Scientist with the Indian Space Research Organisation, Bangalore, India. He has more than 20 years of work experience in the area of digital image processing, geographical information system, software development, and system management. He has worked on geospatial application projects of national missions and large-scale user projects that involved design and development of large database, system integration, and customized solutions. His research interests include digital image processing, mathematical morphology, GISci and geospatial applications, and decision support systems.

Mr. Nagajothi is a member of IEEE GRSS.

B. S. Daya Sagar (M'03–SM'03) received the M.Sc. and Ph.D. degrees in geoengineering and remote sensing from the Faculty of Engineering, Andhra University, Visakhapatnam, India, in 1991 and 1994, respectively.

He is currently a Full Professor with the Systems Science and Informatics Unit (SSIU), Indian Statistical Institute, Bangalore, India. He is also the first Head of the SSIU. From 1992 to 2001, he was with the College of Engineering, Andhra University and the Centre for Remote Imaging Sensing and Processing, The National University of Singapore in various positions. From 2001 to 2007, he was an Associate Professor and Researcher with the Faculty of Engineering and Technology, Multimedia University, Cyberjaya, Malaysia. Since 2017, he has been a Visiting Professor with the University of Trento, Trento, Italy. He has authored/coauthored more than 85 papers in journals, and has authored and/or guest edited 11 books and/or special theme issues for journals. He recently authored a book entitled *Mathematical Morphology in Geomorphology and GISci* (CRC Press, 2013). He recently coedited two special issues on Filtering and Segmentation with Mathematical Morphology for the IEEE JOURNAL OF SELECTED TOPICS IN SIGNAL PROCESSING, and Applied Earth Observation and Remote Sensing in India for the IEEE JOURNAL OF SELECTED TOPICS IN APPLIED EARTH OBSERVATION AND REMOTE SENSING. His recent book *Handbook of Mathematical Geosciences* (Springer, 2018) reached 325 000 downloads. His research interests include mathematical morphology, GISci, digital image processing, fractals and multifractals, their applications in extraction, analyses, and modeling of geophysical patterns.

Dr. Sagar is an Elected Fellow of Royal Geographical Society (1999), Indian Geophysical Union (2011), and was a member of New York Academy of Science during 1995–1996. He is the recipient of the Dr. Balakrishna Memorial Award from Andhra Pradesh Academy of Sciences in 1995, the Krishnan Gold Medal from Indian Geophysical Union in 2002, and the Georges Matheron Award-2011 (with Lecturership) of the International Association for Mathematical Geosciences. He is the Founding Chairman of Bangalore Section IEEE GRSS Chapter. He is on the editorial boards of *Computers & Geosciences*, *Frontiers: Environmental Informatics*, and *Mathematical Geosciences*. He is also the Editor-in-Chief of the Springer Publishers's *Encyclopedia of Mathematical Geosciences*.